Effects of Processing Sequence on Clay Dispersion, Phase Morphology, and Thermal and Rheological Behaviors of PA6-HDPE-Clay Nanocomposites

Mingqian Zhang,[1] Bin Lin,[2] Uttandaraman Sundararaj[2]

[1]*Department of Chemical Engineering, University of Waterloo, Waterloo, Ontario, Canada N2L 3G1*
[2]*Department of Chemical and Petroleum Engineering, University of Calgary, Calgary, Alberta, Canada T2N 1N4*

Received 13 September 2011; accepted 22 December 2011
DOI 10.1002/app.36692
Published online 17 February 2012 in Wiley Online Library (wileyonlinelibrary.com).

ABSTRACT: Effects of processing sequence on the clay dispersion, phase morphology, and thermal and rheological properties of PA6-HDPE-clay nanocomposites are investigated in this study. It has been found that the processing sequence plays a key role in the clay dispersion and phase morphology of the PA6-HDPE-clay nanocomposites. When PA6 is extruded with clay first, either in the absence or presence of HDPE, a continuous PA6 phase domain forms with exfoliated clay platelets that seem to have strong interaction with the dispersed HDPE droplets, leading to a favorable phase morphology. When HDPE is extruded with clay in the first extrusion, nonpolar HDPE molecules are sheared into the clay interlayers and form HDPE intercalated clay, and the HDPE-clay aggregates do not have strong interactions with PA6 in the second extrusion, resulting in a phase morphology of large HDPE particles of hundreds of microns in size dispersed in PA6 phase. The DSC results indicate strong interaction between the polymers and clay; in particular, it is shown there is stabilization of γ-form crystals by the compatibilizer (PEMA). Rheological characterization indicates that the PA6-HDPE-clay nanocomposites exhibit significantly high storage and complex viscosity in the entire frequency range, and the loss modulus of the nanocomposites that have an exfoliated clay dispersion is lower than that of PA6 at high frequency. The results of this study suggest two types of microstructures of the PA6-HDPE-clay nanocomposites are possible using different processing sequences. © 2012 Wiley Periodicals, Inc. J Appl Polym Sci 125: E714–E724, 2012

Key words: clay dispersion; phase morphology; thermal and rheological properties; PA6-HDPE-clay nanocomposites

INTRODUCTION

Polymer nanocomposites based on polyamide 6 (PA6) and polyolefin blends have generated much interest in recent years because of their readily tailored properties.[1–8] PA6 itself is one of the most widely used engineering polymers because of its stiffness and strength, but PA6 has some inherent property shortcomings such as low heat distortion temperature (HDT), high moisture absorption, poor processibility, and it is brittle. In principle, all of these property deficiencies can be improved by blending with low-cost and tough polyolefins such as polypropylene (PP) or polyethylene (PE). The HDT, barrier properties, and mechanical properties of the PA6-polyolefin blends can be further enhanced by the incorporation of nanoscale inorganic fillers such as layered clay during blending process. The underlying rationale of using layered clay as a filler lies in polymer chains penetrating into clay inter layers that are nanometers thick and several hundreds of nanometers wide, resulting in uniformly dispersed clay platelets (intercalated or exfoliated clay) in polymer matrix. The high aspect ratio of nano clay affords high degree of polymer-surface interaction, resulting in greatly improved properties at lower loadings than conventional fillers.[3–8]

The key to enhanced properties for a ternary polymer-polymer-clay nanocomposite such as PA6-PE-clay is proper morphology development between the two polymers and the delamination and dispersion of nanoscale layered clay fillers throughout the polymer matrix. The formation of intercalated or exfoliated clay structure in polymer matrix requires a strong interfacial interaction between the polymers and clay. In general, PA6 is able to easily intercalate into clay layers to form exfoliated clay structure due to strong interaction between PA6 and clay generated by the polarity and hydrogen-bonding capacity. However, most literature on nonpolar PEs has shown that PEs, particularly high density polyethylene (HDPE), exhibit weak interaction with organoclay and so the HDPE-clay composites prepared by conventional melt mixing only have intercalated clay structure.[3,7,9–12] A few recent studies[6–8,12–15] have

Correspondence to: U. Sundararaj (u.sundararaj@ucalgary.ca) or M. Zhang (m78zhang@uwaterloo.ca).

TABLE I
Formulations and Designations of the Nanocomposites in Each Extrusion Step

First extrusion	Second extrusion	Composition	Designation
70% PA6 + 30% PE (M-1)	95% M-1 + 5% clay	66PA/29PE/5clay	AE1
70% PA6 + 30% PE (M-1)	85% M-1 + 10% PEMA + 5% clay	60PA/25PE/10PEMA/5clay	AEM1
93% PA6 + 7% clay (M-2)	71.4% M-2 + 28.6% PE	66PA/29PE/5clay	AE2
80.5% PA6 + 12.7% PEMA + 6.7% clay (M-3)	74.3% M-3 + 25.7% PE	60PA/25PE/10PEMA/5clay	AEM2
85% PE + 15% clay (M-4)	33.4% M-4 + 66.6% PA6	66PA/29PE/5clay	AE3
64.0% PE + 23.5% PEMA + 12.5% clay (M-5)	40.0% M-5 + 60.0% PA6	60PA/25PE/10PEMA/5clay	AEM3

shown that the clay dispersion and phase morphology of PA6-polyolefin-clay nanocomposites are rather complicated, depending on the system composition, clay type, and compatibilizer. It has also been reported for a ternary polymer-polymer-clay nanocomposite that involves two chemically different polymers such as PA6 and PP, the intercalation of one or two polymers into clay interlayers and the overall phase morphology depend on the addition sequence and coalescence. Factors such as composition, rheological and interfacial properties of each component, and processing conditions[4] play an important role in morphology development. As such, it is plausible to expect that the clay dispersion and phase morphology of a ternary PA6-PE-clay system can be kinetically and thermodynamically controlled in continuous mixing process such as extrusion, and thus the processing/mixing sequence can play an important role in clay dispersion, phase morphology, and end-use properties.

In this study, we present a systematic investigation of the effects of processing sequence on clay dispersion, phase morphology, and thermal and rheological properties of PA6-HDPE-clay nanocomposites. A two-step extrusion procedure was applied for the preparation of the nanocomposite samples to ascertain the effects of processing sequence. The influence of compatibilizer on clay dispersion, phase morphology, and thermal and rheological properties is also explored in this study.

EXPERIMENTAL

Materials

Polyamide 6 (PA6) used in this study is a commercial product (Ultramid B40) from BASF with a density of 1.14 g/cm^3. PE is a film-grade high density polyethylene (HDPE, Sclair 19G) supplied by Nova Chemicals, which has a density of 0.96 g/cm^3 and a melt index of 2.0 g/10 min. A maleic anhydride grafted HDPE (EMB-265D) from Dupont was used as a compatibilizer. The organoclay (Cloisite 20A) was obtained from Southern Clay Products.

Preparation of PA6-HDPE-clay nanocomposites

All PA6-HDPE-clay nanocomposites in this study were prepared in a two-step extrusion process using a Coperion 25 mm Mega twin screw corotating extruder, which has a screw diameter of 25 mm and barrel L/D of 37. The extruder was operated at a constant speed of 220 rpm and a barrel temperature in the range of 240–250°C. The total feed rate was about 8 kg/h. These extrusion conditions were employed for both extrusion steps. The extrudate of each extrusion step was cooled using cold water and was fed into a pelletizer to cut the extrudate into small pellets. The pellets were dried thoroughly at 90°C before being used for the second extrusion or for characterization. The formulations and sample designations for each extrusion step are listed in Table I. The final clay content for all samples was 5.0 wt %, and the PEMA content for all nanocomposites with PEMA was 10.0 wt %.

Sample characterization

X-ray diffraction (XRD)

The intercalation of polymers into clay interlayers and clay exfoliation were determined by XRD using a Rigaku diffractometer (Co/K-α1 radiation, λ = 0.1789 nm) at room temperature. The film samples of about 2 mm in thickness made by compression molding were scanned in 2θ ranging from 1° to 11° at a scanning rate of 1°/min.

Transmission electron microscopy (TEM)

Clay dispersion and morphology of nanocomposites were also directly observed by TEM (Philips Morgagni 268 microscope). TEM samples were in the form of thin slice ($\sim$ 100 nm) prepared by microtoming extruded pellets with an Ultracut diamond knife at room temperature. The images of sufficient contrast were measured at an acceleration voltage of 75 kV and are presented without further tainting.

Scanning electron microscopy (SEM)

The phase morphology of the nanocomposite samples was examined by SEM (JEOL JSM-5410 microscope with an acceleration voltage of 75 kV). The SEM observations were performed on either cryogenically fractured surface or ultramicrotomed surface of extruded pellets. All SEM samples were

coated with gold prior to examination under the electron beam.

Differential scanning calorimetry (DSC)

The melting and crystallization behaviors of the nanocomposites were studied under nitrogen atmosphere by DSC on a TA Instrument Model DSC2910. About 10 mg samples cut from the extruded pellets were sealed into aluminum DSC pans and were first heated from 0 to 260°C at a heating rate of 10°C/min and subsequently cooled to 0°C at the same rate. The second heating-cooling cycle was performed right after the first one at the same heating and cooling rates. The melting temperature, crystallization temperature, and enthalpy of fusion were analyzed using TA2200 software package.

Rheological characterization

For rheological characterization, sample disks of 25 mm in diameter and 2 mm in thickness were made by compression molding at about 260°C. A Rheometrics RMS-800 Rheometer was used to measure the elastic modulus (G') and loss modulus (G'') at angular frequency ranging from 0.1 to 100 rad/s. The rheometer was operated at 250°C in an oscillatory mode with 25 mm parallel plate geometry at a gap of 1.5–2.0 mm. Each sample was run at two different gaps or more to ensure the data reproducibility. Prior to the frequency sweep, strain sweeps were performed for each sample to determine the linear viscoelastic regime. All measurements were carried out under nitrogen to minimize polymer degradation and moisture absorption.

RESULTS AND DISCUSSION

Clay structure and dispersion

Figure 1 shows the XRD patterns of the PA6-HDPE-clay nanocomposites prepared from different processing sequences. The XRD pattern of the pure organoclay Cloisite 20A exhibited a broad intense peak at $2\theta = 4.45°$, corresponding to a basal spacing of 2.30 nm. The XRD patterns of the nanocomposite samples vary considerably in comparison to that of the organoclay. For AE2 and AEM2, cases where PA6 was extruded with the clay in the first extrusion, and then the PA6-clay was extruded with HDPE in the second extrusion, the final PA6-HDPE-clay nanocomposites exhibited fully exfoliated clay structure regardless of the presence of PEMA (see the XRD patterns of AE2 and AEM2). Secondly, for AE1 and AEM1 in which PA6 was blended with HDPE in the first extrusion, then the PA6-HDPE blend was extruded with clay in the second extrusion, the clay structure depended on the presence of PEMA in the second extrusion, as shown in Figure 1, the presence of PEMA leaded to fully exfoliated clay structure (AEM1), while the nanocomposite without PEMA showed intercalated clay structure (AE1) with the primary XRD peak of clay shifting to lower angle of around 3.0° and the basal spacing was increased to 3.42 nm. Finally, for AE3 and AEM3 in which the HDPE was extruded with the clay in the absence and presence of PEMA in the first extrusion, and then the HDPE-clay samples were extruded with PA6 in the second extrusion, the clay structure again depended heavily on the presence of PEMA, as shown in Figure 1. The PA6-HDPE-clay sample without PEMA (AE3) showed a intercalated clay structure, with the primary XRD peak of clay shifting to lower angle of around 2.85° and the basal spacing was increased to 3.60 nm, while the final PA6-HDPE-clay with PEMA (AEM3) exhibited fully exfoliated clay structure.

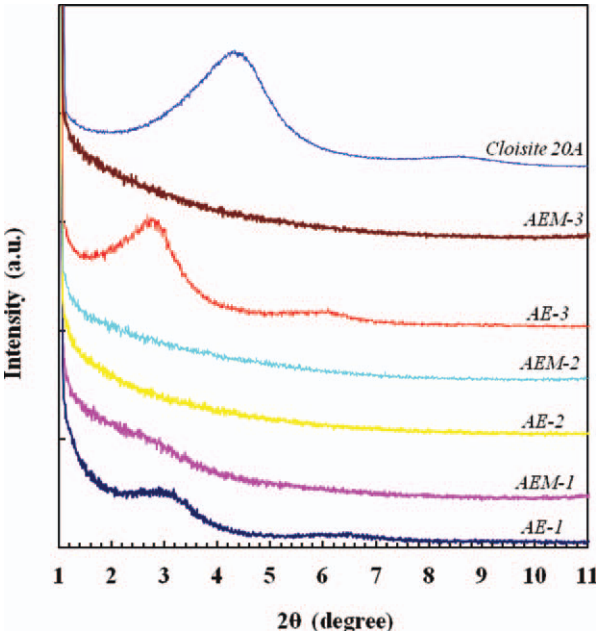

Figure 1 XRD patterns of various PA6-HDPE-clay nanocomposites (samples as denoted in Table I). [Color figure can be viewed in the online issue, which is available at wileyonlinelibrary.com.]

The clay structure and dispersion of the nanocomposites were further verified by TEM. As shown in Figure 2, all the nanocomposite samples with the presence of PEMA (AEM1, AEM2, and AEM3) showed exfoliated clay platelets in polymer matrix, which is in agreement with the XRD results shown in Figure 1. For the nanocomposite samples without PEMA, the TEM images of AE1 and AE3 showed mainly intercalated clay tactoids although exfoliated clay platelets were also visible, whilst AE2 exhibited exfoliated clay. Again these observations are consistent with XRD results. Despite the difference in clay

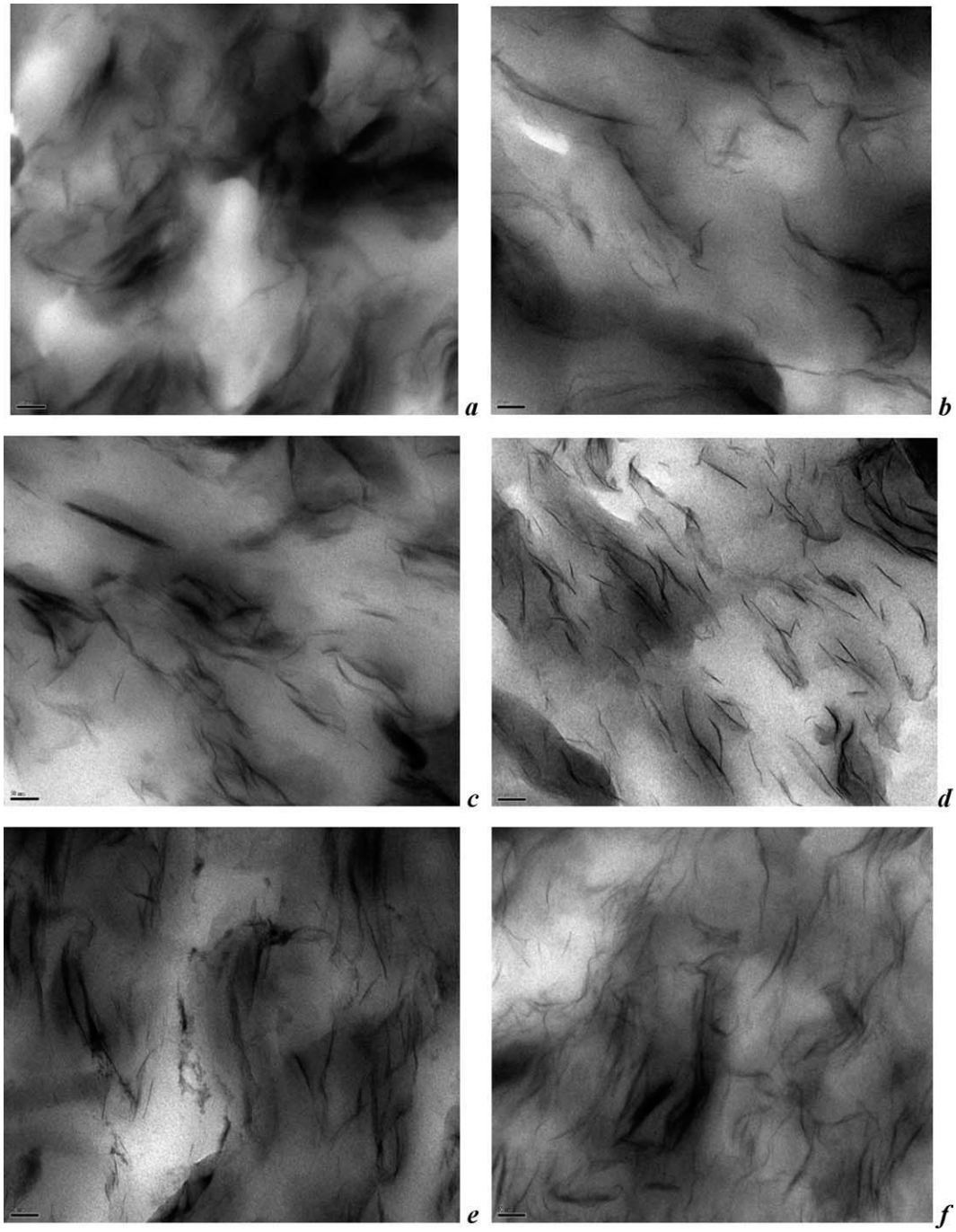

Figure 2 TEM micrographs of various PA6-HDPE-clay nanocomposites: (a) AE1, (b) AEM1, (c) AE2, (d) AEM2, (e) AE3, and (f) AEM3.

structure revealed by XRD analysis, it is important to note that the TEM micrographs of all nanocomposite samples showed very similar distribution of clay platelets or aggregates. Since, the clay compositions, along with the extrusion conditions, are the same for all the like samples, the XRD and TEM results indicate a strong dependence of clay structure and dispersion on processing sequence. It should be mentioned that among the samples of clay out of the first extrusion, PA6-clay (M2), and PA6-PEMA-clay (M3) only showed intercalated clay structure as shown in Figure 3, while HDPE-clay (M4) and HDPE-PEMA-clay (M5) had very little clay intercalation, indicating that the second extrusion is necessary in terms of clay exfoliation.

Phase morphology of nanocomposites

The phase morphology of the PA6-HDPE-clay nanocomposites was examined using SEM. Figure 4

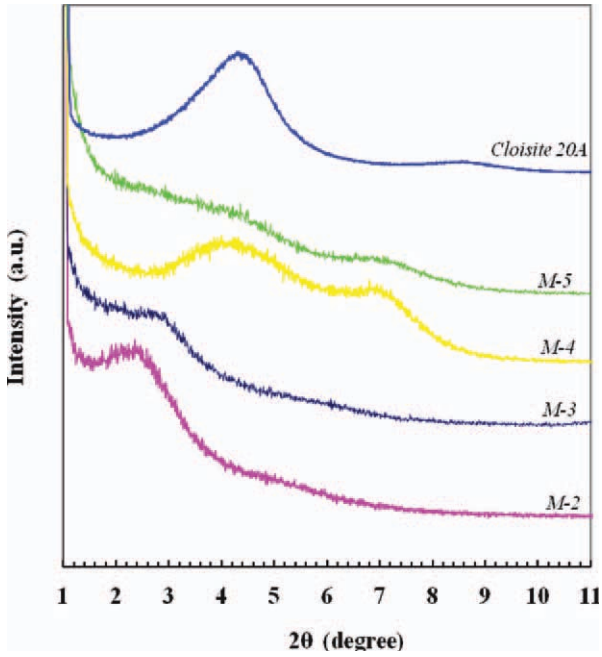

Figure 3 XRD patterns of PA6-clay and HDPE-clay nanocomposites out of the first extrusion (samples as denoted in Table I). [Color figure can be viewed in the online issue, which is available at wileyonlinelibrary.com.]

shows the SEM micrographs of all the nanocomposites. AE1 and AEM1 showed similar morphology of small PE droplets dispersed uniformly throughout continuous PA6 domain, indicating that PEMA seems to have little influence in the formation of the polymer morphology. AE2 and AEM2, prepared by mixing PA6 and clay in the first extrusion step, also showed similar morphology of fine PE droplets dispersed uniformly throughout PA6. However, when HDPE was extruded with the clay in the first extrusion, the presence of PEMA seemed to be effective in the formation of final phase morphology. The nanocomposite in the absence of PEMA (AE3) showed large PE particles sparsely dispersed in PA6 matrix, while the nanocomposite with PEMA (AEM3) showed much smaller PE droplets distributing throughout the continuous PA6 phase.

The XRD, TEM, and SEM results clearly show two types of microstructure of the PA6-HDPE-clay nanocomposites stemming from different processing sequence. When the first extrusion step uses PA6 and clay, the clay tends to be more easily intercalated and the clay platelets are primarily in continuous PA6 phase after the second extrusion step with PE. In particular, the intercalated/exfoliated clay platelets that are uniformly distributed in PA6 phase appear to act as a compatibilizer between PA6 and HDPE, significantly reducing droplet coalescence and resulting in well-dispersed PE phase size, as evidenced in Figure 4. In this case, the effect of the compatibilizer PEMA does not appear to be significant. The promoting effect of organoclay on polymer phase morphology has been observed in other ternary blends such as PA6-PP-clay,[16] PA6-PS-clay,[17] and PA6-clay/mSEBS[18] as well. In contrast, when the first extrusion step uses the HDPE and organoclay, the HDPE intercalated clay aggregates do not seem to be kinetically active with PA6 in the second extrusion process. This leads to poor phase morphology and a microstructure of intercalated clay aggregates mostly in HDPE phase. In this case, the presence of PEMA is effective for promoting clay exfoliation and reducing dispersed phase size.

Thermal characteristics

The thermal characteristics of the PA6-HDPE-clay nanocomposite were studied using DSC cycles of melting and crystallization. Figure 5(a,b) show the DSC endotherms from the first and second heating cycles. There was no visible difference in melting temperature of HDPE among all the samples. As shown in Figure 5(a), PA6 showed two distinct melting peaks, the low-temperature peak at about 210°C is because of the melting of γ-form crystals of PA6, while the high-temperature peak at about 220°C represents α-form crystals of PA6. It is apparent that the α-form crystals dominated all the extruded nanocomposites, as demonstrated by higher peaks of the DSC endotherms of the first heating cycle. However, after the recrystallization of the sample at a cooling rate of 10°C/min, the samples with PEMA showed a transition from the α-form crystals to more stable γ-form crystals, as evidenced by the dominant peaks at lower temperatures in Figure 5(b) for AEM1, AEM2, and AEM3. The samples in the absence of PEMA still showed similar melting curve as those in the first heating cycle.

The striking dependence of the melting behaviors of PA6 on the sample history is a reflection of clay dispersion, thermomechanical history, and cooling conditions of the nanocomposites. It is known that neat PA6 normally crystallizes predominantly in α-form, and the formation of γ-form crystals in PA6-clay nanocomposite is attributed to the γ-nucleation of the clay platelets in the PA6 matrix.[19–21] On the other hand, the shear force from the extrusion process and the subsequent rapid supercooling can cause shear-induced self-nucleation that promotes α-crystallization.[22] The net results of these two competing factors result in the development of more α-form crystals in the extruded samples, as revealed by the DSC endotherms of the first heating cycle in Figure 5(a). After the effect of the mechanical stress is erased by the recrystallization, the samples with PEMA are dominant with γ-form crystals due to the strong interaction of PEMA with clay and PA6, leading to a network structure, which is in favor of the

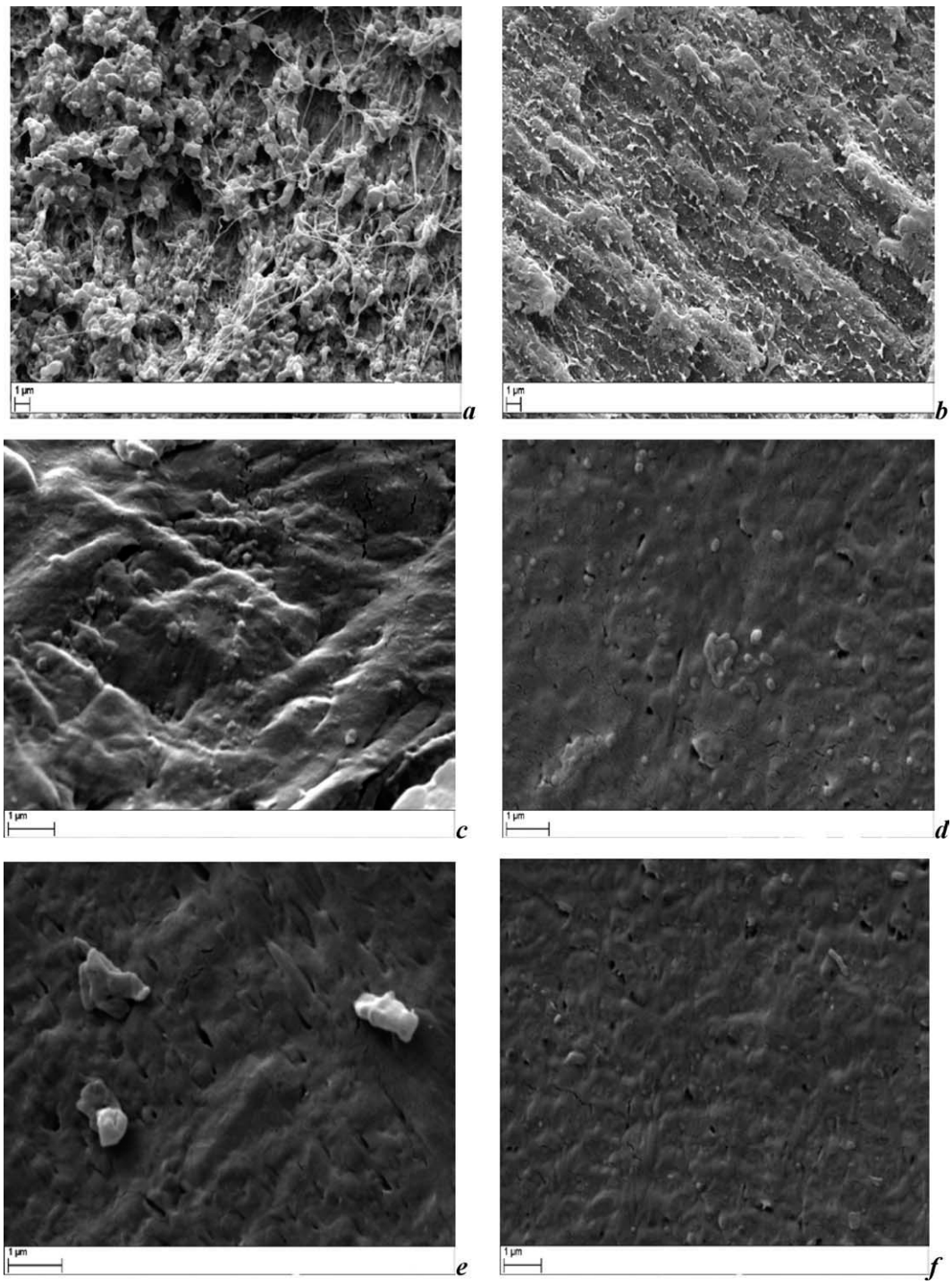

Figure 4 SEM micrographs of various PA6-HDPE-clay nanocomposites: (a) AE1, (b) AEM1, (c) AE2, (d) AEM2, (e) AE3, and (f) AEM3.

γ-form crystals [Fig. 5(b)]. It is important to note that the melting behavior of AE1, AE2, and AE3 are all similar, suggesting that even when HDPE is extruded with clay in the first extrusion for AE3, clay also migrates from PE into PA6 phase. The TEM observation of AE3 in Figure 2 supports this.

To further elucidate the thermal characteristics of PA6-HDPE-clay nanocomposites, the DSC exotherms of PA6 in the nanocomposites, in comparison to that of PA6-HDPE blend prepared under the same conditions, are shown in Figure 6(a). It can be seen that both clay and PEMA influence the crystallization of PA6 in the nanocomposites. As shown in Figure 6(a), the crystallization temperature, T_c, of PA6 in all nanocomposites, was diminished by the addition of the organoclay. The peak T_c for AE1, AE2, and AE3

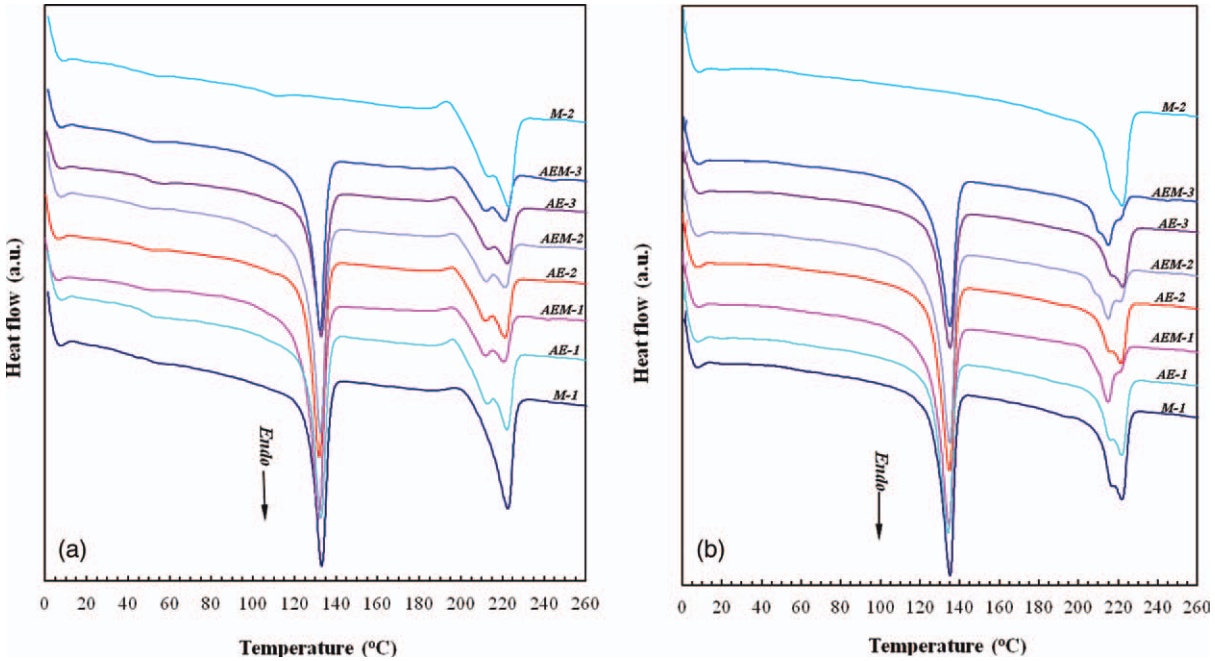

Figure 5 (a) DSC endotherms of PA6-HDPE-clay nanocomposites from first heating cycle. (b) DSC endotherms of PA6-HDPE-clay nanocomposites from second heating cycle. [Color figure can be viewed in the online issue, which is available at wileyonlinelibrary.com.]

decreased to 185, 184, and 183°C as compared to 187.6°C in polymer blend, the peak T_c for AEM1, AEM2, and AEM3 was further decreased to 181, 181.7, and 182.8°C, respectively, in the presence of PEMA. The reduced crystallization temperature is an indicator of the interaction between PA6 and organoclay.[16,19,22] Moreover, as shown above, the organoclay can act as a compatibilizer between PA6 and HDPE, and the formation of a polymer network limits the chain mobility and lowers the crystallization temperature. The presence of PEMA can further reinforce the polymer network and then further diminish the crystallization temperature, leading to more stable γ-form crystals.[21]

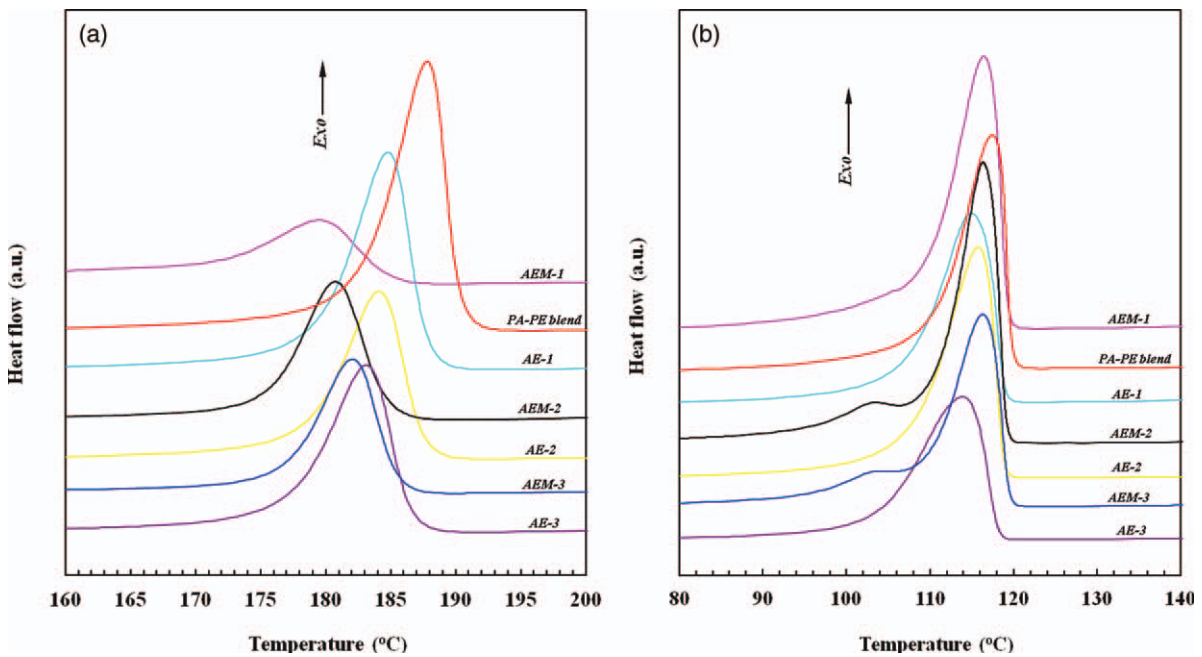

Figure 6 (a) DSC exotherms of the crystallization of PA6 in PA6-HDPE blend and PA6-HDPE-clay nanocomposites. (b) DSC exotherms of the crystallization of HDPE in PA6-HDPE blend and PA6-HDPE-clay nanocomposites. [Color figure can be viewed in the online issue, which is available at wileyonlinelibrary.com.]

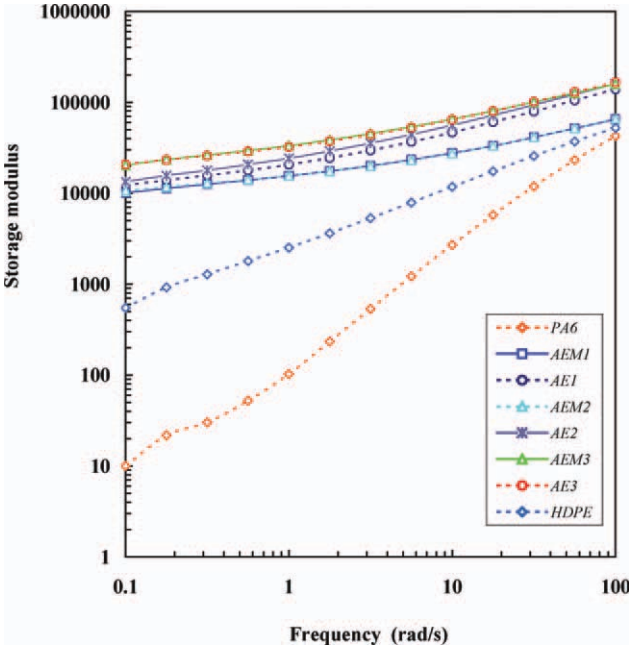

Figure 7 Storage modulus (G') as a function of frequency for PA6-HDPE-clay nanocomposites. [Color figure can be viewed in the online issue, which is available at wileyonlinelibrary.com.]

Figure 6(b) shows the DSC exotherms of HDPE in the nanocomposites in comparison to that of PA6-HDPE blend prepared under the same conditions. The crystallization temperature of HDPE also decreased from 117.5°C in the polymer blend to 114.9, 115.8, and 113.4°C for AE1, AE2, and AE3, respectively. The XRD, TEM, and SEM results showed that the clay dispersion is ordered as AE2 > AE1 ≈ AE3, which is in the same order as the peak crystallization temperature. This implies that the closer the nanocomposite T_c is to that of the PA6-HDPE blend, the stronger is the interaction between HDPE and clay. The peak crystallization temperatures of all three nanocomposites with PEMA were very similar at 116.3°C, and a secondary crystallization existed at about 103°C. It is likely that the formation of the polymer network in the presence of PEMA limits the lamellar thickness of certain HDPE chains.

Rheological properties

Polymer rheological properties are very sensitive to variations in polymer microstructures. For ternary nanocomposites, the compatibility between each polymer and clay will affect the rheological behavior of the composite materials. Dynamic frequency sweep tests on the nanocomposites were conducted to study network formation and microstructural changes of the PA6-HDPE-clay nanocomposites. Figure 7 shows the storage modulus (G') as a function of frequency for neat PA6, neat HDPE, and the PA6-HDPE-clay nanocomposites. It is clearly seen that the viscoelastic behaviors of the nanocomposites are significantly affected by the addition of clay. All nanocomposites, irrespective of clay exfoliation, exhibited significantly higher storage modulus than either of the neat polymers in the entire frequency range. The magnitudes of G' for the nanocomposites in the absence of PEMA were ordered AE3 > AE2 ≈ AE1, and similar trend of G' values was observed for the nanocomposites with PEMA (AEM3 > AEM2 ≈ AEM1).

Figure 8 shows the loss modulus (G'') as a function of frequency for neat PA6, neat HDPE, and the PA6-HDPE-clay nanocomposites. It is seen that the nanocomposites (AE1, AE2, AE3, and AEM3), irrespective of clay exfoliation, exhibited higher loss modulus than either of the neat polymers in entire frequency range. While AEM1 and AEM2 showed lower G'' values than the neat PA6 at frequencies above 11 rad/s. Similar to the trend of G' values, the magnitude of G'' for the nanocomposites in the absence and presence of PEMA were in the order of AE3 > AE2 ≈ AE1 and AEM3 > AEM2 ≈ AEM1, respectively.

It is important to note in Figure 7 that in addition to the increase in the magnitude of G', the slopes of G' of all nanocomposites were smaller than those of the neat polymers. The increase in G' value and the decrease in the slope of G', especially at low-frequency, are indicative of pseudo solid-like behavior at low-frequency and strong interactions between

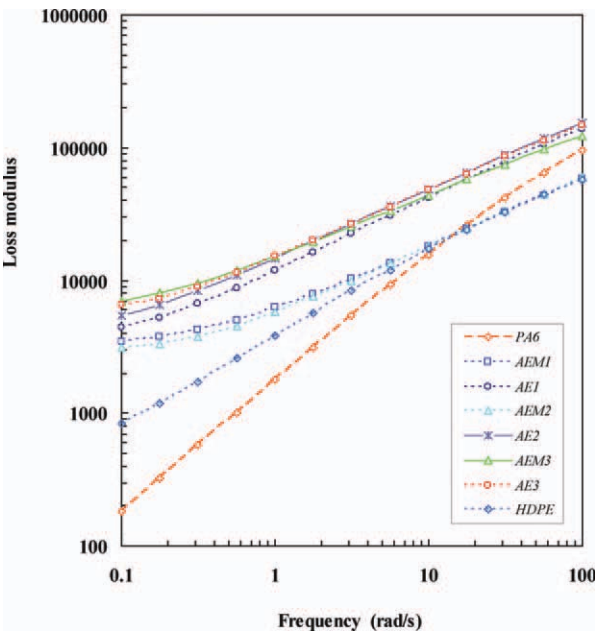

Figure 8 Loss modulus (G'') as a function of frequency for PA6-HDPE-clay nanocomposites. [Color figure can be viewed in the online issue, which is available at wileyonlinelibrary.com.]

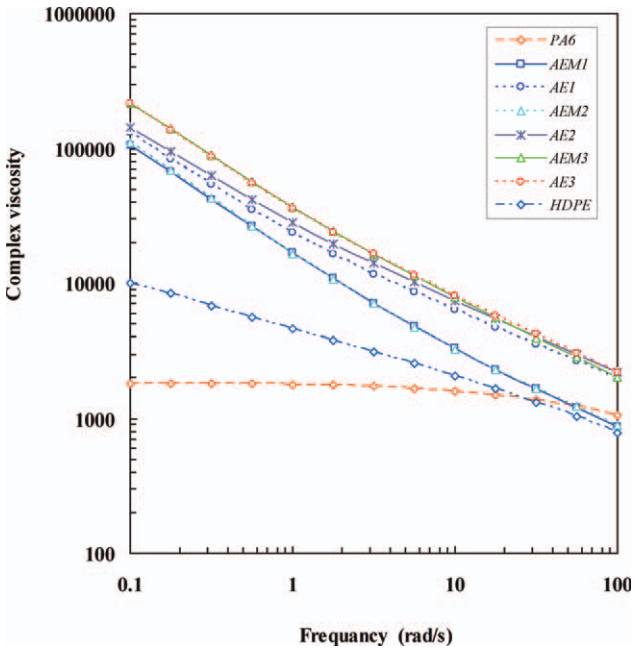

Figure 9 Complex viscosity (η*) as a function of frequency for PA6-HDPE-clay nanocomposites. [Color figure can be viewed in the online issue, which is available at wileyonlinelibrary.com.]

clay and polymer phase.[7,23,24] It has been established in the literature that the higher the absolute G' value and the smaller the slope, the better dispersed are the clay platelets in polymer matrix.[23,24] Highly dispersed clay with excellent interaction with polymers can lead to a supermolecular or network structure formation in the nanocomposites.[19,23] To further elucidate the relation between clay dispersion and rheological behavior, the complex viscosity (η*) as a function of frequency for neat PA6, neat HDPE, and the HDPE-PA6-clay nanocomposites are plotted in Figure 9. Neat PA6 shows Newtonian plateau at low-frequency, while the HDPE showed shear thinning. The complex viscosities of the nanocomposites were much higher than those of the neat polymers, and showed a much stronger shear thinning effect than HDPE in the entire frequency range, as indicated by the steeper slopes in Figure 9. The drastically increased dynamic viscosities at low-frequency indicate that the clay platelets are well dispersed for all nanocomposites including those with intercalated clay structure. It is possible that the clay platelets or tactoids orient in shear direction when subjected to shear. As the shear rate increases, the increased alignment of clay in shear direction substantially reduces the viscosity.

The effect of clay dispersion on rheological behavior can be semiquantitatively analyzed by a power-law relation between complex viscosity, η*, and frequency, ω;$\eta^* = k\omega^n$ where k is a sample specific preexponential factor and n is the shear thinning exponent. The value of k and n can be directly obtained from the logarithmic plot of η* versus ω as, $\log(\eta^*) = \log(k) + n\log(\omega)$

The shear thinning exponent, n, is the slope and a semiquantitative measure of the clay dispersion in polymer phase.[23] The values of n for the nanocomposites, along with the terminal η* values, are listed in Table II. It can be seen that all the nanocomposites exhibited an excellent linear relation between logarithmic complex viscosity and logarithmic frequency, as indicated by the value of R^2. The values of n for the nanocomposites in the absence of PEMA are greater than those of their counterparts in the presence of PEMA, indicating the better clay dispersion and thus more shear thinning resulting from interfacial interaction of PEMA. The values of n for AE1 and AE2 are similar, as are those of AEM1 and AEM2, suggesting these pairs have similar clay dispersion or network structure. This is in agreement with the results of XRD, TEM, and SEM. It is intriguing to see that terminal viscosity of AE3 is higher than that of AE2 or AE1 and the n-value of AE3 is lower than that of AE2 and AE1. This observation cannot be simply explained by the clay dispersion because AE1 and AE2 had much better clay dispersion than AE3, as revealed by XRD and TEM. One plausible explanation is the intercalation of HDPE molecules into clay interlayers, which results from shear intercalation during the first extrusion step. The HDPE intercalated clay can render similar interaction between polymer and clay as the exfoliated clay, and may offer certain macroscopic property advantages.[25]

The above analysis suggests that two types of microstructures can arise for the PA6-HDPE-clay nanocomposites from different processing sequences. The first microstructure, arising from PA6 and clay in the first extrusion and HDPE in the second extrusion, consists of clay platelets or aggregates mainly dispersed in PA6 phase and some platelets at the interphase of PA6 and HDPE, as shown in

TABLE II
Terminal Viscosities and Shear Thinning Exponent of the PA6-HDPE-Clay Nanocomposites

Sample	η* (ω = 0.1) (kPa s)	η* (ω = 100) (kPa s)	$-n$	R^2
PA6	1.830	1.050	0.070	0.7944
HDPE	9.990	0.777	0.363	0.9972
AE1	130	1.97	0.599	0.9927
AEM1	107	0.870	0.699	0.9951
AE2	144	2.21	0.599	0.9956
AEM2	111	0.889	0.701	0.9935
AE3	217	2.22	0.660	0.9945
AEM3	216	2.00	0.675	0.9967

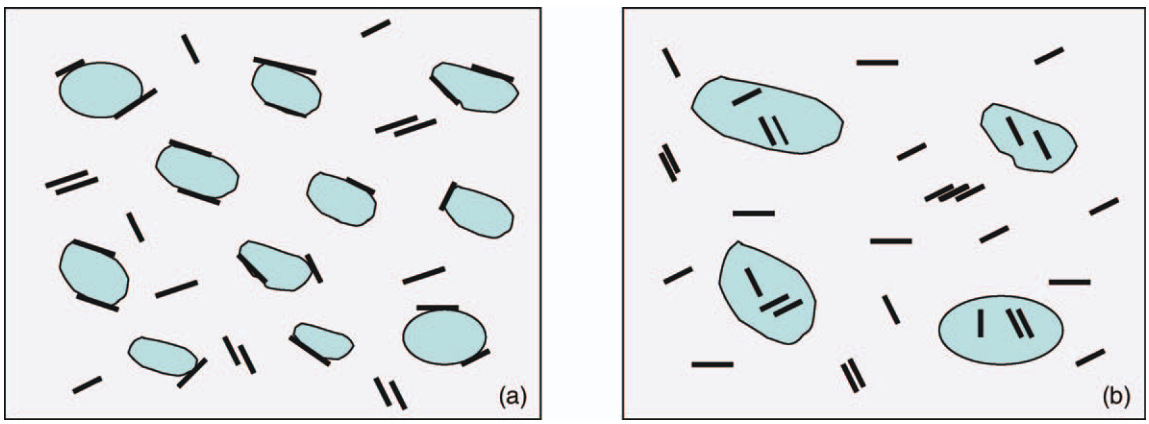

Figure 10 Schematic diagram of two types of microstructures for PA6-HDPE-clay nanocomposites (PA6: continuous phase; HDPE: dispersed phase). (a) PA6 and clay in the first extrusion and HDPE added in the second extrusion (b) HDPE and clay in the first extrusion and PA6 added in second extrusion. [Color figure can be viewed in the online issue, which is available at wileyonlinelibrary.com.]

diagram A in Figure 10. The network structure shows excellent clay dispersion and favorable phase morphology (AE1 and AE2). The second microstructure, arising from HDPE and clay in the first extrusion and PA6 in second extrusion, has HDPE intercalated clay and clay platelets or aggregates in PA6 phase, as shown in diagram B in Figure 10, resulting in good clay dispersion but unfavorable phase morphology (AE3). We expect that the two microstructures would render different end-use properties, as indicated by the rheological properties.

CONCLUSIONS

Different PA6-HDPE-clay nanocomposites were prepared by a two-step extrusion process. It was found that the processing sequence plays an important role in the clay dispersion, phase morphology, and thermal and rheological properties of the PA6-HDPE-clay nanocomposites. When PA6 is extruded with clay and even in the presence of HDPE in the first extrusion, the resultant PA6-HDPE-clay nanocomposites have a continuous PA6 phase domain with exfoliated clay platelets and fine HDPE droplets dispersed in the continuous phase. The exfoliated clay appears to promote the favorable polymer blend phase morphology and the effect of compatibilizer PEMA is insignificant. When HDPE is extruded with the clay in the first extrusion, the nonpolar HDPE molecules are sheared into clay interlayers and form HDPE intercalated clay, it seems that the PE-clay aggregates have little interaction with PA6 in the second extrusion, leading to phase morphology of larger HDPE particles dispersed in PA6 phase. The DSC results show considerably different melting and crystallization behaviors of both PA6 and HDPE in the nanocomposites when compared to DSC scans of neat PA6 and HDPE, suggesting a strong interaction between each polymer and clay, which is strongly supported by the stabilization of γ-form crystals of PA6 by PEMA in the nanocomposites. Rheological characterization indicates that the PA6-HDPE-clay nanocomposites exhibit significantly high storage and complex viscosity in the entire frequency range, and the loss modulus of the nanocomposites with exfoliated clay dispersion and PEMA is lower than that of PA6 at high-frequency. The rheological results also corroborate that two types of microstructures of the PA6-HDPE-clay nanocomposites stems from different processing sequences, and will perhaps lead to different end uses for these nanocomposites.

References

1. Campoy, I; Arribas, J. M.; Zaporta, M. A. M.; Marca, C.; Gomez, M. A.; Fatou, J. G. Eur Polym J 1995, 31, 475.
2. Ohlsson, B.; Hassander, H.; Tornell, B. Polymer 1998, 39, 4715.
3. Mehrabzadeh, M.; Kamal, M. R. Can J Chem Eng 2002, 80, 1083.
4. Wahit, M. U.; Hassan, A.; Rahmat, A. R.; Mohd Ishak, Z. A. J Elastomers Plast 2006, 38, 231.
5. Wahit, M. U.; Hassan, A.; Mohd Ishak, Z. A.; Rahmat, A. R.; Abu Bakar, A. J Thermoplast Compos Mater 2006, 19, 545.
6. Contreas, V.; Cafiero, M.; Da Silva, S.; Rosales, C.; Perera, R.; Matos, M. Polym Eng Sci 2006, 46, 1111.
7. Filippone, G.; Dintcheva, N. Tz.; Acierno, D.; La Mantia, F. P. Polymer 2008, 49, 1312.
8. Kusmono, Z. A.; Mohd Ishak, Z. A.; Chow, W. S.; Rochmadi, T. T. Polym Eng Sci 2010, 50, 1493.
9. Mehrabzadeh, M.; Kamal, M. R. Polym Eng Sci 2004, 44, 1152.
10. Zhong, Y.; Janes, D.; Zheng, Y.; Hetzer, M.; Kee, D. D. Polym Eng Sci 2007, 47, 1101.
11. Spencer, M. W.; Cui, L.; Yoo, Y.; Paul, D. R. Polymer 2010, 51, 1056.
12. Scaffaro, R.; Botta, L.; Mistretta, M. C.; La Mantia, F. P. Polym Degrad Stab 2010, 95, 2547.
13. Chow, W. S.; Mohd Ishak, Z. A.; Karger-Kocsis, J.; Apostolov, A. A.; Ishiaku, U. S. Polymer 2003, 44, 7427.

14. Chiu, F.; Fu, S.; Chuang, W.; Sheu, H. Polymer 2008, 49, 1015.
15. Erdmann, E.; Dias, M. L.; Pita, V. J. R. R.; Destefanis, H.; Monasterio, F.; Acosta, D. Macromol Symp 2007, 258, 82.
16. Wang, H.; Zeng, C.; Elkovitch, M.; Lee, L. J.; Koelling, K. W. Polym Eng Sci 2001, 41, 2036.
17. Kelnar, I.; Rotrekl, J.; Kotek, J.; Kapralkova, L.; Hromadkova, J. Eur Polym J 2009, 45, 2760.
18. Gonzalez, I.; Eguiazabal, J. I.; Nazabal, J. Eur Polym J 2008, 44, 287.
19. Chiu, F.; Lai, S.; Chen, Y.; Lee, T. Polymer 2005, 46, 11600.
20. Mathias, L. J.; Davis, R. D.; Jarrett, W. L. Macromolecules 1999, 32, 7958.
21. Devaux, E.; Bourbigot, S.; El Achari, A. J Appl Polym Sci 2002, 86, 2416.
22. Miri, V.; Elkoun, S.; Peurton, F.; Vanmansart, C.; Lefebvre, J. M.; Krawceak, P.; Seguela, R. Macromolecules 2008, 41, 9234.
23. Durmus, A.; Kasgoz, A.; Macosko, C. W. Polymer 2007, 48, 4492.
24. Huitric, J.; Ville, J.; Mederic, P.; Moan, M.; Aubry, T. J Rheol 2009, 53, 1101.
25. Zhang, M.; Sundararaj, U. Macromol Mater Eng 2006, 291, 697.